2966–2971 *Nucleic Acids Research, 1999, Vol. 27, No. 14*

Packaging of DNA by shell crosslinked nanoparticles

K. Bruce Thurmond II, Edward E. Remsen[1], Tomasz Kowalewski and Karen L. Wooley*

Department of Chemistry, Washington University, 1 Brookings Drive, St Louis, MO 63130, USA and
[1]Monsanto Company, 800 North Lindbergh, St Louis, MO 63167, USA

Received February 4, 1999; Revised and Accepted May 24, 1999

ABSTRACT

We demonstrate compaction of DNA with nanoscale biomimetic constructs which are robust synthetic analogs of globular proteins. These constructs are ~15 nm in diameter, shell crosslinked knedel-like (SCKs) nanoparticles, which are prepared by covalent stabilization of amphiphilic di-block co-polymer micelles, self-assembled in an aqueous solution. This synthetic approach yields size-controlled nanoparticles of persistent shape and containing positively charged functional groups at and near the particle surface. Such properties allow SCKs to bind with DNA through electrostatic interactions and facilitate reduction of the DNA hydrodynamic diameter through reversible compaction. Compaction of DNA by SCKs was evident in dynamic light scattering experiments and was directly observed by *in situ* atomic force microscopy. Moreover, enzymatic digestion of the DNA plasmid (pBR322, 4361 bp) by *Eco*RI was inhibited at low SCK:DNA ratios and prevented when ≤60 DNA bp were bound per SCK. Digestion by *Msp*I in the presence of SCKs resulted in longer DNA fragments, indicating that not all enzyme cleavage sites were accessible within the DNA/SCK aggregates. These results have implications for the development of vehicles for successful gene therapy applications.

INTRODUCTION

Biomimicry (1,2), which relies upon guidance from biology and biotechnology in the design of novel synthetic or natural materials, is emerging as an effective strategy in diminishing the size of devices while maintaining their complex functionality. Since the size of many functional biological structures falls in the 10–100 nm range, it is appropriate to seek methods for preparation of functional analogs within the newly developing field of nanotechnology. Herein, we present a novel approach for mimicking the basic features of globular proteins, such as their overall size, shape and surface charge. This approach relies on self-assembly of amphiphilic synthetic di-block copolymers into globular core–shell nanostructures, followed by stabilization via covalent crosslinking. Since crosslinking occurs selectively within the shell of assembled polymer micelles, these novel constructs are referred to as shell crosslinked knedel-like (SCK) nanospheres. (*Knedel* is a polish term for dumplings, having a spherical shape and core–shell morphology. For synthetic nanomaterials of similar morphology see 3.) Owing to their amphiphilic core–shell morphology, SCKs belong to the same category as globular amphiphilic biological nanostructures such as lipoproteins, viruses, globular proteins, etc., in broad physicochemical terms. These synthetic constructs could prove to be important for biomedical applications, particularly those involving gene delivery and expression.

Handling of long DNA chains within the limited space available in cells is facilitated by various compaction mechanisms (4–6). Several synthetic systems, including liposomes (7–9), linear polymers (10,11), cationic lipid–peptoid conjugates (12), polymer micelles (13,14), dendrimers (15) and organic nanoparticles (16–18) have been shown to bind DNA and provide protection against enzymatic digestion. The non-particulate nature of liposomes and linear polymers apparently results in the complexation of DNA through non-specific electrostatic interactions leading to a heterogeneous binding character (8,9,11). Polymer micelles typically exist with diameters of 10–100 nm and they possess a core–shell morphology that can contain cationic surface charges, however, the micellar organization is a self-assembled structure that can be easily deformed or destroyed during complexation with DNA due to the absence of covalent stabilization. Other known globular macromolecular entities, such as dendrimers, are covalently bound macromolecules, but they are not readily synthesized to 10 nm diameters (19,20). Previously studied organic nanoparticles were typically >>50 nm with broad size distributions. Herein, we report the interaction of DNA with stable, synthetic SCKs (shown schematically in Fig. 1) of ~15 nm diameter (3), which is intermediate between the sizes available for dendrimers and organic nanoparticles. We also illustrate the effect of compaction on the accessibility of DNA toward the action of digestive enzymes and show evidence of DNA release from the DNA/nanoparticle complexes.

MATERIALS AND METHODS

Materials

DNA plasmid pBR322, *Eco*RI, *Msp*I, NEBuffer 1, NEBuffer 2, pBR322 DNA *Msp*I digest and Lambda DNA *Bst*EII digest were purchased from New England BioLabs (Beverly, MA) and used as received. Tris base (Sigma), sodium acetate

*To whom correspondence should be addressed. Tel: +1 314 935 7136; Fax: +1 314 935 4481; Email: klwooley@artsci.wustl.edu
Present address:
K. Bruce Thurmond II, Monsanto Company, 800 North Lindbergh, St Louis, MO 63167, USA

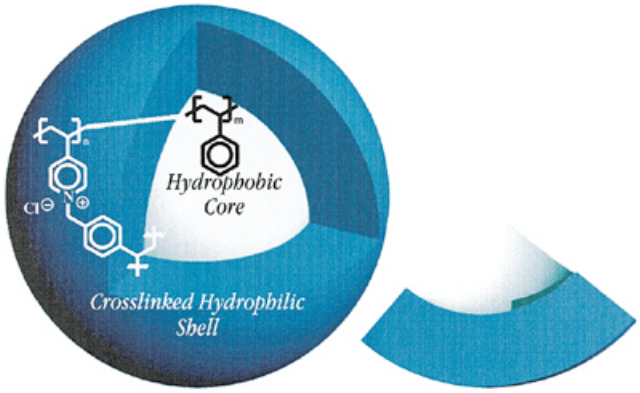

Figure 1. Schematic representation of the shell crosslinked knedel-like (SCK) nanosphere, containing a crosslinked, positively charged, hydrophilic shell layer surrounding the hydrophobic core domain. The SCKs are prepared from assembly of block co-polymers of polystyrene and *p*-chloromethylstyrene-quaternized poly(4-vinyl pyridine) into polymer micelles, followed by crosslinking through reaction of the styrenyl moieties located within the shell.

(Sigma), EDTA dihydrate (Sigma) and agarose (Fisher) were used as received. The experimental details for the preparation of the SCK nanospheres are described elsewhere (21). The SCK composition consisted of a polystyrene (PS) core encapsulated within a layer of poly(4-vinyl pyridine) (PVP) that had been quaternized with 4-chloromethylstyrene to provide crosslinking throughout the shell layer. The ratio PS:PVP was 1:2, with 46% of the pyridyl nitrogens quaternized by reaction with 4-chloromethylstyrene (21).

General procedure for the cleavage of pBR322 with *Eco*RI in the presence of SCK

Complexes A–C were prepared by mixing 1 µl pBR322 (1 µg/µl), 1, 3 or 5 µl SCKs (8×10^{-6} M) and 1 µl HEPES (1 M). Total volumes were raised to 10 µl with doubly distilled water if the restriction enzyme was not added. If restriction enzyme was to be added, the total volume was raised to 8.8 µl with doubly distilled water and 1 µl 10× NEBuffer 1 and 0.2 µl *Eco*RI (20 000 U/ml) were added. The samples were incubated at 37°C for 3 h, vacuum centrifuged for ~5 min and 6 µl of 2× gel loading buffer were added. Samples were analyzed by electrophoresis at 55–65 V for 2–2.5 h with a 1% agarose gel in 1× acetate buffer. DNA was visualized with ethidium bromide (1 µg/ml of gel).

General procedure for timed digestion experiments

Complexes A–C were prepared at four times the volume by mixing 4 µl pBR322 (1 µg/µl) with 4, 12 or 20 µl SCKs (8×10^{-6} M). Total volumes were raised to 35.2 µl with doubly distilled water. An aliquot of 4 µl of 10× NEBuffer 1 was added to each sample, followed by addition of 0.8 µl *Eco*RI (20 000 U/ml). The samples were incubated at 37°C with aliquots removed at the specified intervals. After removal of the last aliquot, 6 µl of 2× loading buffer were added to each sample. Samples were analyzed by electrophoresis at 55–65 V for 2–2.5 h with a 1% agarose gel in 1× acetate buffer. DNA was visualized with ethidium bromide (1 µg/ml of gel). Controls were run on the same gel under the same conditions. Spot densitometry of the DNA on the gel was made using the NIH shareware tnimage (http://las1.ninds.nih.gov/pub/unix/).

General procedure for the cleavage of pBR322 with *Msp*I in the presence of SCK

Formation of complex A has been described. Complex D was prepared by mixing 1 µl pBR322 (1 µg/µl), 0.5 µl SCK (8×10^{-6} M) and 1 µl HEPES (1 M). Total volumes were raised to 10 µl with doubly distilled water if the restriction enzyme was not added. If restriction enzyme was to be added, 1 µl of 10× NEBuffer 2 was added to each sample, followed by addition of 0.8 µl *Msp*I (20 000 U/ml). The samples were incubated at 37°C for 3 h, vacuum centrifuged for ~5 min and 6 µl of 2× gel loading buffer were added. Marker solutions consisted of 1.5 µl of marker and 6 µl of 2× gel loading buffer. Samples were analyzed by electrophoresis at 55–65 V for 2–2.5 h with a 1% agarose gel in 1× acetate buffer. DNA was visualized with ethidium bromide (1 µg/ml of gel).

Measurement of melting curve of DNA and SCK/DNA complexes

Melting transitions were measured upon aqueous solutions of DNA and an SCK/DNA complex with a molar ratio of 80:1. DNA melting curves were obtained in a Cary 1e at 260 nm with a heating rate of 5°C/15 min (the temperature was raised 5°C and allowed to equilibrate for 15 min) from 50 to 90°C.

Atomic force microscopy (AFM) of SCK/DNA complexes

All AFM observations were carried out with the aid of a Nanoscope III-M system (Digital Instruments, Santa Barbara, CA) equipped with a vertical engage J-scanner. The imaging conditions were as follows: TESP tapping mode silicon cantilevers (nominal spring constant 50 N/m, typical resonance frequency in the range 250–300 kHz); cantilever oscillation amplitude 0.5 V (non-calibrated signal); set-point corresponding to 95% of free oscillation amplitude; scan frequency 3 Hz; integral gain 0.7, proportional gain 5.0 (instrument settings in arbitrary units).

The sample was prepared by placing a 2 µl drop of solution containing DNA (10 µg/ml, 4.6 kb circular luciferase expression vector) and SCKs in 10 mM HEPES, 2 mM $MgCl_2$, pH 7.6, on a surface of freshly cleaved mica (New York Mica Company, New York, NY); after ~5 s, necessary for binding of the DNA and SCKs to the mica, the excess solution was washed away with 200 µl of ultrapure water and the surface was dried under a stream of nitrogen.

Tapping mode imaging under buffer was performed using a standard contact mode fluid cell and 100 µm, wide legged, silicon nitride cantilevers (nominal spring constant 0.58 N/m). The cantilever was oscillated by applying a sinusoidal voltage across the Z-direction of the scanner (22), which required minor modification of the controller electronics, performed according to the manufacturer's instructions. Best results were obtained when the cantilever was driven at a frequency range corresponding to the broad maximum of cantilever oscillation amplitude centered around 8–9 kHz (23–25). Imaging conditions were as follows: cantilever oscillation amplitude signal (uncalibrated) 0.5–1.0 V; set-point corresponding to above 90% of free oscillation amplitude; integral and proportional gains 0.3 and 2.0 (instrument settings in arbitrary units); scan frequency 1–4 Hz.

Samples for imaging under liquid were prepared in a 10 mM HEPES, 1.5 mM $ZnCl_2$, pH 7.6, buffer. A 30–40 µl drop of SCK–DNA solution was placed directly on the working surface of a fluid cell, which was then positioned on the scanner. Imaging was carried out after several minutes, which was necessary for equilibration of the solution in contact with the mica.

Dynamic light scattering (DLS) of SCK/DNA complexes

The DLS instrumentation was a Brookhaven Instruments Co. (Holtsville, NY) system containing a model BI-200SM goniometer, a model EMI-9865 photomultiplier and a model BI-9000AT digital correlator. Incident light was provided by a model 95-2 Ar ion laser (Lexel Corp., Palo Alto, CA) operated at 514.5 nm. All measurements were made at 20°C. Prior to analysis, solutions were centrifuged in a model 5414 microfuge (Brinkman Instrument Co., Westbury, NY) for 6 min to sediment dust.

Scattered light was collected at a fixed angle of 90°. The digital correlator was operated with 200 channels, a dual sampling time of 100 ns, a 5 µs ratio channel spacing and a duration of 5 min. A photomultiplier aperture of 200 µm was used and the incident laser intensity was adjusted to obtain a photon counting rate of 83 000 c.p.s. Only measurements in which measured and calculated baselines of the intensity autocorrelation function agreed to within 0.1% were used to calculate particle size. The calculation of particle size distribution and distribution averages was performed with the ISDA software package (Brookhaven Instruments Co., Holtsville, NY) which employed single exponential fitting, cumulants analysis and non-negatively constrained least squares particle size distribution analysis routines (26).

RESULTS AND DISCUSSION

SCKs, which are essentially stabilized polymer micelles, are constructed by a combination of covalent and non-covalent interactions to readily build up spherical polymer nanoparticles of the appropriate size and chemical composition for interaction with DNA. The SCKs are prepared in a three-step process, including: (i) the synthesis of a linear amphiphilic block copolymer; (ii) self-assembly into spherical micelles in aqueous solution; (iii) stabilization by intramicellar crosslinking of functionalities located within the shell domain. The SCKs used in this study consisted of hydrophobic PS cores and hydrophilic, crosslinked *p*-chloromethylstyrene-quaternized PVP shells (21). SCKs prepared from polymer chains of 20 700 Da molecular weight and a ratio of PS:PVP repeat units of 1:2 have a solid-state diameter of 9 ± 3 nm and a hydrodynamic diameter of 16 ± 2 nm, determined by AFM and DLS, respectively. The positive charges, an average of 500 per SCK, are located throughout the several nanometer thick shell, so that all cations are not expected to be accessible for strong interaction with the DNA phosphate ester anions.

The aggregation of DNA with SCKs was studied by a combination of AFM (27,28), DLS and enzymatic digestion experiments. Initial evidence of adhesive interaction between SCKs and plasmid DNA was obtained from AFM observations of dehydrated samples adsorbed on mica, which revealed the presence of bulky aggregates of the SCKs with partially exposed segments of unbound DNA (Fig. 2). These aggregates markedly differed from aggregates of SCKs on mica in the absence of DNA. Typical morphologies of aggregates of free SCKs, depending on concentration of starting solution, ranged from scattered single particles (26) through monolayer patches (3) to uniform films (data not shown). It is important to note that SCKs in complexes with DNA maintained their original size and shape. However, the supercoiled form of the DNA appears to have been perturbed in some regions. Further confirmation of the supercoiling perturbation of plasmid complexed with SCKs was obtained from the UV/vis spectroscopic studies of DNA melting; thermal denaturation of the plasmid alone occurred at 75°C, whereas the melting temperature of the DNA was lowered to 70°C in Complex B.

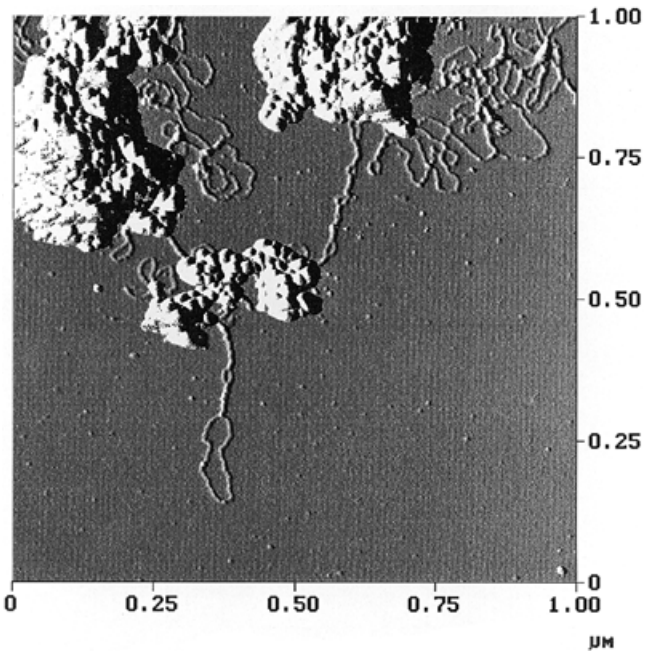

Figure 2. Tapping mode AFM image of DNA/SCK aggregates dried on the surface of mica, demonstrating SCK/DNA binding with maintenance of the SCK size and shape. Some regions exhibit unbound DNA, while others display SCKs bound along the DNA in a similar fashion as previously observed in AFM images of chromatin (31).

Further insights into the mechanism of compaction were obtained from *in situ* AFM experiments carried out under solution with increasing ratios of SCK:DNA plasmid (pBR322, 4361 bp). As illustrated in Figure 3A, at a SCK:DNA molar ratio of 20:1 (as in Complex A) the majority of DNA was still in the unbound supercoiled state. This can be understood by bearing in mind that despite the large molar excess of SCKs at this stoichiometry, the charge ratio between SCK and DNA plasmid just reaches the value of 1:1. (The ratio of charges is determined from the *p*-chloromethylstyrene quaternization extent of the PVP SCK shell material, which gives cationic sites, and assuming two negative charges per base pair.) At higher SCK:DNA molar ratios, more compact complexes, such as those shown in Figure 3B (globular aggregate with some DNA loops still visible outside) and in Figure 3C (globular complex with no DNA visible) were observed.

DLS measurements (29) confirmed that the SCK/DNA aggregates formed while in solution and provided for

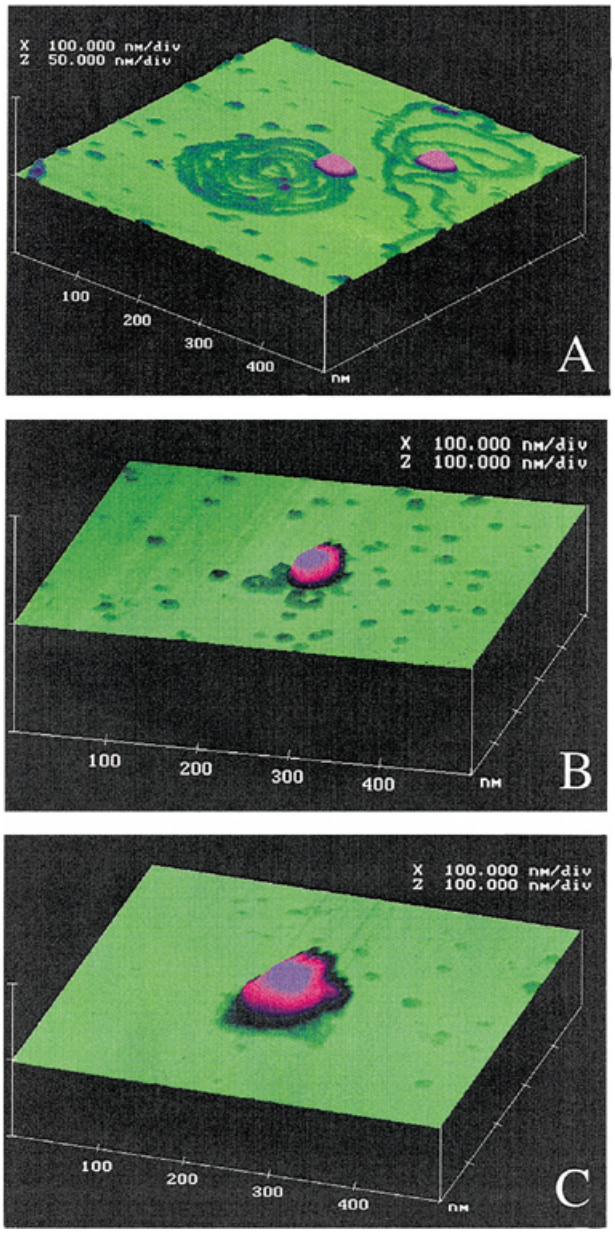

Figure 3. *In situ* tapping mode AFM images of aggregates of SCKs with DNA (pBR322, 4361 bp) adsorbed on freshly cleaved mica and visualized under buffer (10 mM HEPES, 1.5 mM $ZnCl_2$, pH 7.6). (**A**) SCK bound to the plasmid DNA (2 nM SCK, 0.1 nM DNA, molar ratio as in complex A; see Table 1); (**B**) a globular aggregate with loops of DNA still visible (8 nM SCK, 0.1 nM DNA); (**C**) large SCK/DNA aggregate with no identifiable DNA (8 nM SCK, 0.1 nM DNA). The presence of Zn^{2+} in the buffer used for *in situ* imaging was necessary to facilitate attachment of DNA/SCK complexes to mica (32). In control experiments with DNA alone, in which weaker binding Mg^{2+} was used, DNA was observed to change position on the surface from scan to scan. Under similar conditions, complexes of SCKs with DNA were bound to the surface more weakly than DNA alone and their bulky character made them more susceptible to displacement by the AFM tip.

determination of the average diameter values for the aggregates (Table 1). The mean volume-weighted hydrodynamic diameters (D_m) increased by at least a factor of four ($D_{m,i}/D_{m,SCK}$) for each of the complexes in comparison to SCK, suggesting

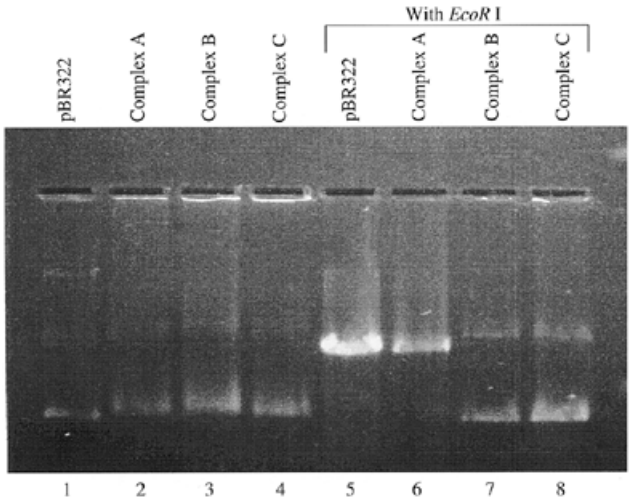

Figure 4. Complexation of pBR322 with SCK offers protection from *Eco*RI digestion. The DNA and DNA/SCK complexes (A–C) were incubated for 3 h at 37°C in the absence (lanes 1–4) and presence (lanes 5–8) of *Eco*RI.

that the interactions between DNA and SCK produce complexes that are multimeric in SCK.

The hydrodynamic diameter distribution of the DNA used to prepare SCK/DNA complexes was also characterized by DLS. Unlike the SCK component of the complexes, the diameter distribution of the DNA component was extremely broad. The broad size range of DNA molecules apparent in the DLS results is consistent with the heterogeneity found in electrophoresis gels of the DNA; the plasmid and its cleaved forms are observed and each is expected to adopt many conformations that are non-spherical and that can lead to a continuous size distribution rather than discrete entities. Diameters ranged from 15 to >3000 nm, with a calculated intensity-weighted mean diameter of 562 nm. In contrast, diameters of all the SCK/DNA complexes were <300 nm (Table 1) and of lower size dispersity.

The accessibility of the DNA within the SCK/DNA complexes was evaluated by enzyme digestion experiments, using a restriction endonuclease, *Eco*RI, and was found to be dependent on the extent of aggregation. As illustrated in Figure 4, the DNA/SCK complexes are destroyed during gel electrophoresis (lanes 2–4) and unbound DNA is observed, which provides a method for analysis of DNA cleavage under the action of enzymes. It is important to note that this release of the DNA, which is a prerequisite for gene therapy applications, is unique to SCKs. Each of the previously studied systems listed above have shown binding to DNA, but no apparent release of the DNA, observed as reduced DNA mobility upon gel electrophoresis. Upon incubation in the presence of *Eco*RI for 3 h at 37°C, the unbound DNA and the loosely bound DNA/SCK complex (Complex A) allowed for complete cleavage of the supercoiled plasmid to an open linear form (lanes 5 and 6, respectively), whereas Complexes B and C offered protection to the DNA (lanes 7 and 8, respectively).

Timed digestion experiments revealed that while all SCK/DNA complexes inhibited DNA cleavage, inhibition time increased with an increase in the molar ratio of SCK:DNA.

Table 1. SCK/DNA complexes studied and the hydrodynamic diameter distribution data from dynamic light scattering[a]

Complex	Molar ratio (SCK:DNA)	Charge ratio (SCK:DNA)	Base pairs per SCK	D_1[b] (nm)	V_1 (vol%)	D_2[b] (nm)	V_2 (vol%)	D_m[c] (nm)	$D_{m,i}/D_{m,SCK}$[d]
A	20	1:1	200	36	80	280 ± 170	20	85	4.9
B	70	4:1	60	120	>99	<5	<1	120	6.7
C	120	7:1	40	26	85	120 ± 32	15	40	2.4
SCK alone	–	–	0	15	99	>100	1	16	1.0

[a]All measurements were made at 20°C and reported hydrodynamic diameters and volume % are mean values of two determinations.

[b]Diameter distributions were calculated from autocorrelation functions of light scattering intensities using a multiple pass non-negatively constrained least squares fitting (NNLS) algorithm in the ISDA software package from Brookhaven Instruments Co. (Holtsville, NY). A bimodal distribution of particles was observed, with diameters D_1 and D_2 for volume fractions V_1 and V_2.

[c]D_m is the volume-averaged mean particle or aggregate diameter, calculated as $D_m = (D_1 \cdot V_1 + D_2 \cdot V_2)/(V_1 + V_2)$.

[d]$D_{m,i}/D_{m,SCK}$ is the ratio of D_m values for the complexes versus the D_m value of the SCK, where i = A, B or C.

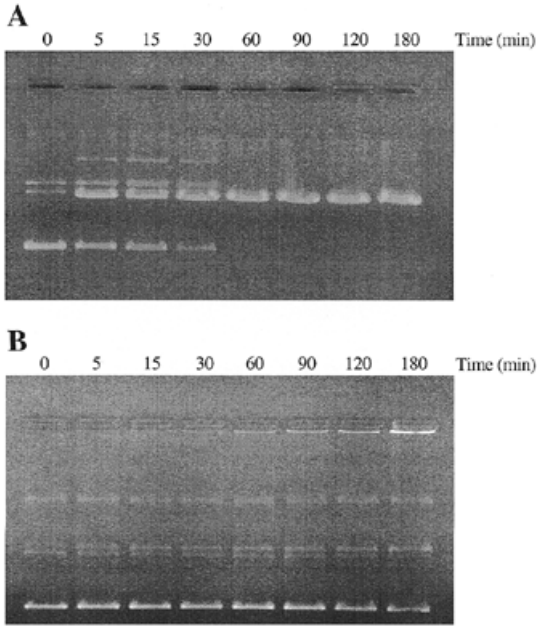

Figure 5. Cleavage of pBR322 by *Eco*RI is inhibited at low SCK content and is prevented at high SCK content. (**A**) Complex A incubated with *Eco*RI for 0–180 min. Cleavage of all DNA occurred by 60 min. (**B**) Complex C incubated with *Eco*RI for 0−180 min. No measurable cleavage products are observed.

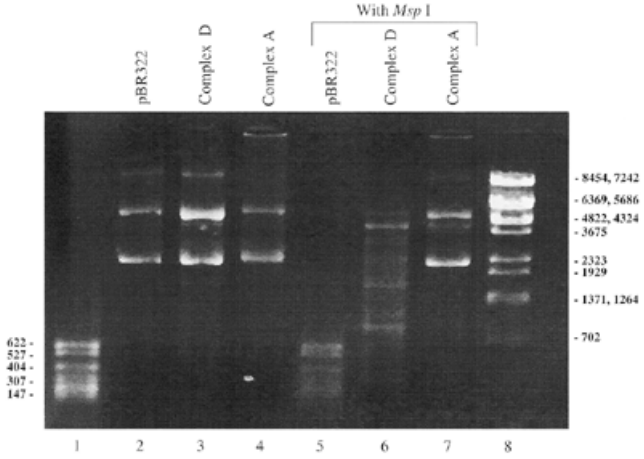

Figure 6. A portion of sites are not accessible to enzymatic digestion when the digestion is performed with *Msp*I (a restriction endonuclease that cleaves pBR322 at 26 sites) upon pBR322 in the presence of SCKs. Even with a 180 min incubation time, cleavage is prevented for Complex A (lane 7). Cleavage of the DNA of Complex D (SCK:DNA molar ratio 12:1, charge ration 0.7:1) results in less extensively fragmented DNA (lane 6) than found for *Msp*I digestion of pBR322 without the SCK nanoparticles present (lane 5). Lane 1 is the marker pBR322 DNA *Msp*I digest and lane 8 is the marker Lambda DNA *BstE*I digest.

Digestion was entirely prevented at the SCK:DNA molar ratio of 70:1 (60 bp per SCK). Representative gels for the digestion experiments with low and high SCK content are shown in Figure 5. For Complex A, the disappearance of the supercoiled DNA plasmid corresponds to the appearance of the cleaved DNA (Fig. 5A). In contrast, for Complex C (Fig. 5B), disappearance of supercoiled DNA does not lead to an increase in the amount of cleaved DNA, instead, at longer incubation times extensive aggregation of residual material in the well is observed.

Further evidence for protection of SCK-compacted DNA was obtained with *Msp*I, a restriction endonuclease that cleaves pBR322 at 26 sites. At SCK:DNA ratios that provide for inhibition but still allow for partial DNA digestion, the lengths of the majority of DNA cleavage products were slightly larger than 702, 1371 and ~3675 bp (Fig. 6, lane 6), whereas unprotected DNA was cleaved into lengths of ≤622 bp (Fig. 6, lane 5). The increased lengths of the degradation products is expected to result from interaction of the DNA with the SCKs, thus limiting the number of sites that are accessible to the enzyme, and is perhaps an indication of a selective binding mode.

We have demonstrated that synthetic functional nanostructures that are designed to exhibit just the basic physicochemical attributes (size, shape persistence and surface charge) of proteins involved in DNA compaction can effectively compact DNA and protect it from enzymatic digestion.

Importantly, these novel constructs maintain their size and shape upon complexation and they are also capable of releasing the DNA, in analogy with biological systems. The observed protection of SCK-compacted DNA can be explained as an effect of enclosure of DNA within the bulk of aggregates. Experiments with short, linear DNA fragments are expected to reveal whether SCKs are capable of binding and protecting DNA by a mechanism that involves selective binding at a single particle level, which would make them even closer mimics of DNA compacting proteins such as histones. SCKs show promise as synthetic nanoparticulate compacting agents for control of DNA accessibility and may find applications in gene transfection and expression. They offer the additional unique advantages of a well-defined structure and modifiable surface chemistry (3) to target site-specific delivery routes.

ACKNOWLEDGEMENTS

We thank Professor John-Stephen Taylor for helpful discussions and Dr Mu Wang for technical assistance. Christopher G. Clark Jr is acknowledged for preparation of Figure 1. This work was supported by the National Science Foundation (K.L.W.) and by the NIH (T.K.).

REFERENCES

1. Choi,S.-K., Mammen,M. and Whitesides,G.M. (1997) *J. Am. Chem. Soc.*, **119**, 4103–4111.
2. Felgner,P.L. (1997) *Sci. Am.*, **276**, 102–106.
3. Thurmond,K.B., Kowalewski,T. and Wooley,K.L. (1996) *J. Am. Chem. Soc.*, **118**, 7239–7240.
4. Polach,K.J. and Widom,J. (1995) *J. Mol. Biol.*, **254**, 130–149.
5. Studitsky,V.M., Kassavetis,G.A., Geiduschek,E.P. and Felsenfeld,G. (1997) *Science*, **278**, 1960–1963.
6. Luger,K., Mäder,A.W., Richmond,R.K., Sargent,D.F. and Richmond,T.J. (1997) *Nature*, **389**, 251–260.
7. Behr,J.-P. (1994) *Bioconjug. Chem.*, **5**, 382–389.
8. Lasic,D.D., Strey,H., Stuart,M.C.A., Podgornik,R. and Frederik,P.M. (1997) *J. Am. Chem. Soc.*, **119**, 832–833.
9. Koltover,I., Salditt,T., Rädler,J.O. and Safinya,C.R. (1998) *Science*, **281**, 78–81.
10. Kabanov,A.V., Astafieva,I.V., Maksimova,I.V., Lukanidin,E.M., Georgiev,G.P. and Kabanov,V.A. (1993) *Bioconjug. Chem.*, **4**, 448–454.
11. Yoshikawa,K., Yoshikawa,Y., Koyama,Y. and Kanbe,T. (1997) *J. Am. Chem. Soc.*, **119**, 6473–6477.
12. Huang,C.-Y., Uno,T., Murphy,J.E., Lee,S., Hamer,J.D., Escobedo,J.A., Cohen,F.E., Radhakrishnan,R., Dwarki,V. and Zuckermann,R.N. (1998) *Chem. Biol.*, **5**, 345–354.
13. Katayose,S. and Kataoka,K. (1997) *Bioconjug. Chem.*, **8**, 702–707.
14. La,S.B., Okano,T. and Kataoka,K. (1996) *J. Pharm. Sci.*, **85**, 85.
15. Baker,J.R.,Jr, Bielinska,A., Johnson,J., Yin,R. and Kukowska-Latallo,J.F. (1996) In Felgner,P.L., Heller,M.J., Lehn,P., Behr,J.P. and Szoka,F.C.,Jr (eds) *Artificial Self-assembling Systems for Gene Delivery*. American Chemical Society, Washington, DC, pp. 129–145.
16. Fritz,H., Maier,M. and Bayer,E. (1997) *J. Colloid Interface Sci.*, **195**, 272–288.
17. Maruyama,A., Ishihara,T., Kim,J.S., Kim,S.W. and Akaike,T. (1997) *Bionconjug. Chem.*, **8**, 735–742.
18. Truong-Le,V.U.L., August,J.T. and Leong,K.W. (1998) *Hum. Gene Ther.*, **9**, 1709–1717.
19. Gauthier,M., Tichagwa,L., Downey,J.S. and Gao,S. (1996) *Macromolecules*, **29**, 519–527.
20. Hawker,C.J. (1997) *Acc. Chem. Res.*, **30**, 373–382.
21. Thurmond,K.B.,II, Kowalewski,T. and Wooley,K.L. (1997) *J. Am. Chem. Soc.*, **119**, 6656–6665.
22. Hansma,P.K., Cleveland,J.P., Radmacher,M., Walters,D.A. and Hillner,P.E. (1994) *Appl. Phys. Lett.*, **64**, 1738–1740.
23. Kasas,S., Thomson,N.H., Smith,B.L., Hansma,H.G., Zhu,X., Guthold,M., Bustamante,C., Kool,E.T., Kashlev,M. and Hansma,P.K. (1997) *Biochemistry*, **36**, 461–468.
24. Lyubchenko,Y. and Shlyakhtenko,L. (1997) *Proc. Natl Acad. Sci. USA*, **94**, 496–501.
25. Yip,C. and Ward,M. (1996) *Biophys. J.*, **71**, 1071–1078.
26. Stock,R.S. and Ray,W. (1985) *J. Polym. Sci. Polym. Phys.*, **23**, 1393–1447.
27. Hansma,H.G., Golan,R., Hsieh,W., Lollo,C.P., Mullen-Ley,P. and Kwoh,D. (1998) *Nucleic Acids Res.*, **26**, 2481–2487.
28. Dunlap,D.D., Maggi,A., Soria,M.R. and Monaco,L. (1997) *Nucleic Acids Res.*, **25**, 3095–3101.
29. Huang,H., Kowalewski,T., Remsen,E.E., Gertzmann,R. and Wooley,K.L. (1997) *J. Am. Chem. Soc.*, **119**, 11653–11659.
30. Tatchell,K. and Van Holde,K.E. (1978) *Proc. Natl Acad. Sci. USA*, **75**, 3583–3587.
31. Martin,L.D., Vesenka,J.P., Henderson,E. and Dobbs,D.L. (1995) *Biochemistry*, **34**, 4610–4616.
32. Hansma,H.G. and Laney,D.E. (1996) *Biophys. J.*, **70**, 1933–1939.